PHYSICAL REVIEW APPLIED 6, 011001 (2016)

Efficient Extraction of Zero-Phonon-Line Photons from Single Nitrogen-Vacancy Centers in an Integrated GaP-on-Diamond Platform

Michael Gould,[1,*] Emma R. Schmidgall,[2] Shabnam Dadgostar,[3] Fariba Hatami,[3] and Kai-Mei C. Fu[1,2]

[1]*Department of Electrical Engineering, University of Washington, Seattle, Washington 98195, USA*
[2]*Department of Physics, University of Washington, Seattle, Washington 98195, USA*
[3]*Department of Physics, Humboldt-Universitat zu Berlin, Newtonstrasse 15, 12489 Berlin, Germany*

(Received 13 June 2016; published 29 July 2016)

Scaling beyond two-node quantum networks using nitrogen-vacancy (NV) centers in diamond is limited by the low probability of collecting zero-phonon-line (ZPL) photons from single centers. Here, we demonstrate GaP-on-diamond disk resonators which resonantly couple ZPL photons from single NV centers to single-mode waveguides. In these devices, the probability of a single NV center emitting a ZPL photon into the waveguide mode after optical excitation can reach 9%, due to a combination of resonant enhancement of the ZPL emission and efficient coupling between the resonator and waveguide. We verify the single-photon nature of the emission and experimentally demonstrate both high in-waveguide photon numbers and substantial Purcell enhancement for a set of devices. These devices may enable scalable integrated quantum networks based on NV centers.

DOI: 10.1103/PhysRevApplied.6.011001

The negatively charged nitrogen-vacancy (NV) center in diamond shows significant promise as a solid-state qubit register [1–3] for measurement-based quantum-information processing (MBQIP) [4–6]. The computational resource in MBQIP is a network of entangled qubit registers. For NV centers, this network can be grown via single-photon measurement of the NV zero-phonon line (ZPL) emission [7,8]. Two-qubit networks of NV centers have been heralded in this manner using free-space collection optics [9,10]. However, the demonstrated entanglement generation rate was significantly slower than the electron spin decoherence rate, and thus far too slow to allow multiqubit entanglement. The limiting factor in reported entanglement rates is the low probability of detecting a ZPL photon upon excitation of an NV center. We will call this probability the total quantum efficiency η. Successful entanglement is heralded by two independent ZPL photon detection events [11], and thus the entanglement generation rate scales as η^2. Low achieved η values are primarily the result of two effects inherent to NV centers in diamond. First, the high refractive index of diamond limits free-space collection efficiency through total internal reflection. Second, phonon interactions result in only ~3% of radiative emission occurring via the ZPL transition [12–14]. Photonic device integration can mitigate both effects, providing a scalable photonics platform for building quantum networks.

In this Letter, we demonstrate a key step toward realizing such a network in a GaP-on-diamond integrated photonics platform: the efficient optical coupling of single NV centers to single-mode waveguides. We show that the probability of emitting a ZPL photon into the guided mode after optical excitation can reach 9%. This high probability is achieved through a combination of resonant enhancement of ZPL emission via the Purcell effect [15], as well as efficient coupling between the resonant devices and waveguides. Resonantly enhanced waveguide collection rates which exceed the theoretical limit for nonresonant collection were exhibited by 10 out of 80 tested devices. The limiting factor for yield is the NV-cavity coupling which can be readily improved with NV-cavity registration. Furthermore, the devices were fabricated on the same chip as passive integrated photonic components [16] necessary for on-chip entanglement generation networks. Combined, these results indicate the promise of the GaP-on-diamond photonics platform for scalable quantum networks.

Our platform utilizes a 125-nm-thick GaP membrane to guide optical modes at the surface of a diamond chip [12,16], taking advantage of the high refractive index of GaP ($n = 3.3$) compared with that of diamond ($n = 2.4$). This is in contrast to the more common approach utilizing the diamond itself as the waveguiding material [17]. A key advantage of the hybrid platform is fabrication scalability. Specifically, diamond waveguides require either undercutting of the diamond [18,19] or working with thin diamond membranes on a low index substrate [20,21]. Undercutting requires a three-dimensional dry etch, significantly constraining the device layout. Thin diamond membranes with large area and uniformity have yet to be demonstrated, resulting in poor device uniformity across a chip. On the other hand, large-area (cm-scale) highly uniform GaP membranes can be grown epitaxially and transferred to bulk single-crystal diamond chips, enabling the fabrication of large numbers of photonic devices with

*gouldm2@uw.edu

good cross-chip uniformity. For complex photonic circuits, additional features of the GaP-on-diamond platform include the introduction of a second-order optical nonlinearity [22], which should enable active photonic routing, and sub-nm top-surface roughness suitable for the development of on-chip superconducting nanowire single-photon detectors [23–25]. The primary disadvantage associated with the hybrid-material platform is the inherently weaker coupling between the emitters located in the diamond and the guided optical modes primarily localized in the GaP. However, as we demonstrate below, this effect is mitigated with resonant devices of sufficiently high quality factor.

The photon-collection devices consist of near-surface NV centers evanescently coupled to the fundamental TE-polarized whispering-gallery mode of 1.3-μm-diameter disk resonators. The resonators are coupled to 150-nm-wide single-mode ridge waveguides [Figs. 1(a) and 1(b)]. Prior to device fabrication, near-surface NV centers were created in the single-crystal electronic-grade diamond chip by nitrogen ion implantation and annealing. A 125-nm GaP membrane was then transferred onto the diamond via epitaxial lift-off and van der Waals bonding [26]. Devices were fabricated on the resulting GaP-on-diamond chip by electron-beam lithography and reactive ion etching [27]. The resulting device cross section is a 125-nm GaP waveguiding layer on a 600-nm diamond pedestal, with a sparse layer of NV centers ($\sim 2 \times 10^9$ cm^{-2}) in the top 10–20 nm of the diamond. Further fabrication details are given in the Supplemental Material [28,29].

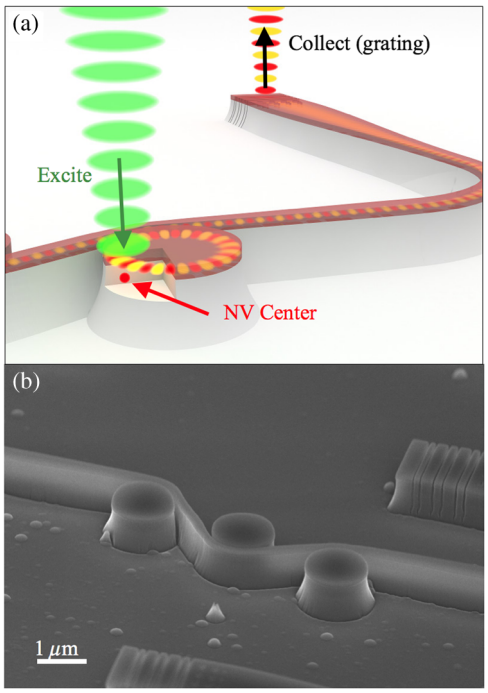

FIG. 1. (a) Illustration of device measurement showing grating collection. (b) Scanning-electron-microscope image of fabricated devices.

Measurements are performed with the fabricated devices cooled to 8 K. For each device, the resonator mode is first tuned to the ZPL resonance. Tuning is accomplished via xenon gas deposition, which causes the cavity modes to redshift and provides a wavelength tuning range of ~2 nm. For cavity tuning measurements, the sample is excited at normal incidence and fluorescence spectra are collected from the output grating coupler as illustrated in Fig. 1(a). An example tuning curve which shows clear NV-cavity coupling as the cavity is tuned to the NV ZPL resonance is shown in Fig. 2(a). This initial tuning measurement is performed on approximately 80 devices expected to lie within the cavity tuning range of the ZPL wavelength, for four different excitation locations around the perimeter of each disk. In this way, a subset of devices showing coupled ZPL emission is identified for further study. Three additional types of measurements are performed on devices in this subset: photon autocorrelation ($g^{(2)}$) on the grating-coupled ZPL emission to confirm the single-photon nature of the collected fluorescence, power dependence to determine saturated collection rates, and lifetime measurements to quantify the resonant enhancement of the ZPL emission.

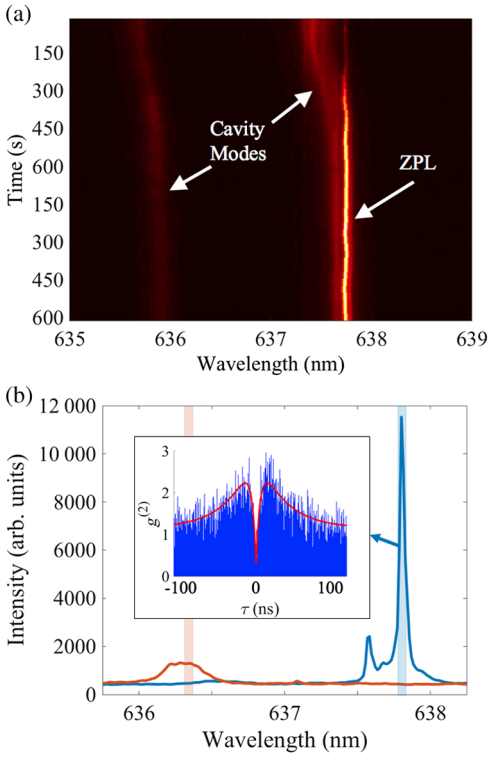

FIG. 2. (a) Measured tuning curve showing two cavity modes as one is tuned onto resonance with a coupled NV center's ZPL. (b) Grating-collected spectra with cavity tuned onto selected ZPL (blue curve) and detuned from ZPL (orange curve), with the wavelength integration range used for count-rate calculation indicated by shaded rectangles. Inset: photon autocorrelation measured with cavity tuned onto ZPL, with the biexponential fit shown in red.

As we show below, the last two measurements enable two separate estimates of η for each device.

With a cavity mode tuned onto resonance with a selected ZPL, we first perform a $g^{(2)}$ measurement to verify the single-emitter nature of the source [see inset Fig. 2(b)]. The grating-collected light is spectrally filtered around the selected ZPL wavelength before detection as depicted in Fig. 2(b). The $g^{(2)}$ measurement is performed on four of the brightest devices, all showing autocorrelation dips with $g^{(2)}(0) < 0.4$, indicating that in each device a majority of the collected photons are from a single emitter. Nonzero coincidence rates are the result of background fluorescence at the ZPL wavelength. This background fluorescence can be observed in the detuned-cavity spectrum (orange) in Fig. 2(b).

We next measure the excitation power dependence of the waveguide-coupled ZPL photon rate to determine saturated collection rates. This measurement is performed by sweeping the excitation power and measuring the grating-coupled detection rate, again spectrally filtered around the selected ZPL. After removal of the background fluorescence, measured with the cavity mode detuned from the ZPL, the data are fit to a saturation model: $\gamma(P) = \gamma_{\mathrm{sat}}/(1 + P/P_{\mathrm{sat}})$, where $\gamma(P)$ is the detection rate, γ_{sat} is the saturated detection rate, P is the excitation power, and P_{sat} is the saturation power.

Power dependence data for four devices are shown in Fig. 3 (inset). Disk 1 shows a detected ZPL count rate of 1.2×10^4 s^{-1} after background subtraction. The fit indicates a saturated NV ZPL detection rate of 2.0×10^4 s^{-1}, and a saturation power of 3.4 mW. Using the measured collection path efficiency for each device [28] and the known detector efficiency, we can estimate the saturated collection rate into the bus waveguide. In the case of disk 1, the estimated on-chip collection rate is 2.5×10^6 s^{-1} from a single saturated NV center. Figure 3 shows a histogram of saturated on-chip collection rates for 10 devices with values exceeding 5×10^5 s^{-1}. We note that the estimated count rates for the three brightest devices are comparable to the best reported collection rates of NV ZPL photons into guided modes for all-diamond devices [20]. All 10 devices exhibit on-chip ZPL count rates exceeding the theoretical limit of approximately 3×10^5 s^{-1} in the absence of Purcell enhancement, calculated as 3% of a total saturated emission rate of 1×10^7 s^{-1} [30].

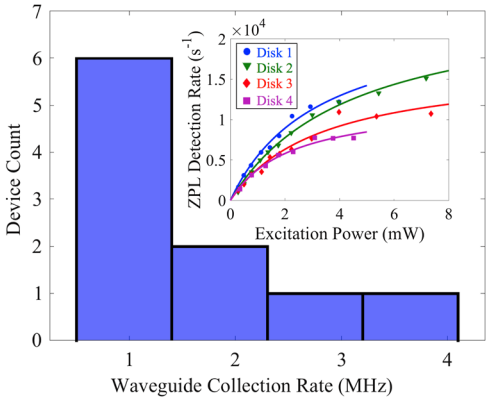

FIG. 3. Histogram of estimated saturated collection rates into bus waveguides for ten devices. Inset: power dependence of on-resonance NV ZPL detection rate for four selected devices, with background removed. Solid lines are fits to the saturation model.

In order to quantify the achieved Purcell enhancement, the excited-state lifetimes of individual NV centers are measured using a directly modulated laser diode [31] with a measured fall time of 1 ns. Time-resolved measurements are taken on disks 1-4, with the cavity on resonance with a selected ZPL, as well as off resonance. After careful subtraction of the background fluorescence waveform [28,32,33], the data are fit to exponential decay curves to obtain the lifetimes. Figure 4 depicts measured on- and off-resonance time-resolved photoluminescence curves for disks 1 and 2. Measured lifetimes under both resonance conditions are compared in order to determine the Purcell enhancement factor F_P of a given device. In the nonresonant case, the lifetime τ_0 is determined by $1/\tau_0 = \Gamma_0 = \Gamma_{\mathrm{ZPL}} + \Gamma_{\mathrm{PSB}}$, in which Γ_{ZPL} (Γ_{PSB}) is the emission rate into the ZPL (phonon sidebands). In the resonant case, the lifetime τ_{res} is determined by $1/\tau_{\mathrm{res}} = \Gamma_{\mathrm{res}} = (1 + F_P)\Gamma_{\mathrm{ZPL}} + \Gamma_{\mathrm{PSB}}$. For disk 1, the measured on-resonance lifetime of 4.7 ± 0.4 ns is significantly shorter than the off-resonance lifetime of 8.7 ± 0.8 ns, with the ratio corresponding to a resonant Purcell factor of $F_P = 26$. This is close to the maximum possible $F_{P,\mathrm{max}} \approx 30$ for this device geometry, given a measured quality factor of $Q = 8200$ [27]. We note that the off-resonance lifetimes in all four measured devices are significantly shorter than the NV lifetime in bulk diamond (~12 ns) [34,35]. The shorter lifetimes are consistent with a broadband enhancement effect caused by the NV centers' proximity to the diamond-GaP interface [28,36].

The total quantum efficiency η is estimated for disks 1–4 by two different methods. In the first method, the measured on-resonance lifetime is used to estimate the total saturated

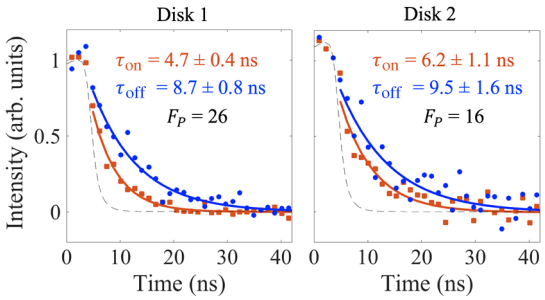

FIG. 4. Fluorescence lifetime measurements for disks 1 and 2, in both the resonant (orange) and off-resonant (blue) conditions. Thick lines represent exponential fits. The dashed black line is the measured system response for reflected excitation light.

emission rate γ_{tot} of a selected NV center [28,37,38]. For a saturated on-chip collection rate of γ_{wg}, η_1 is given by

$$\eta_1 = \frac{\gamma_{wg}}{\gamma_{\text{tot}}}. \quad (1)$$

In the case of disk 1, $\eta_1 \approx 9\%$. The second method uses the total quantum efficiency into the disk resonator mode η_{disk}, calculated from the measured Purcell enhancement factor, and the disk-to-waveguide out-coupling efficiency, determined from grating-coupled transmission measurements [28]. In this case,

$$\eta_2 = \eta_{\text{out}}\eta_{\text{disk}} = \frac{\eta_{\text{out}}F_P}{F_P + \Gamma_0/\Gamma_{\text{ZPL}}}, \quad (2)$$

where η_{out} is the disk-to-waveguide out-coupling efficiency and $\Gamma_0/\Gamma_{\text{ZPL}} \approx 30$. For disk 1, $\eta_2 \approx 9\%$. Table I summarizes the estimated total quantum efficiency obtained using both methods for four devices, showing reasonable agreement between the two.

We have shown that large η values are achievable in a GaP-on-diamond platform, using devices that can be readily integrated into larger on-chip photonic networks. A reasonable excitation repetition rate for NV-NV entanglement is 100 kHz, limited by the NV initialization time [10]. The demonstrated collection efficiency of 9% would thus limit NV-NV entanglement generation to a rate of 400 Hz, which significantly exceeds the ~1-s electron spin decoherence rate [39]. Achieving this efficiency-limited entanglement rate will require that all waveguide-coupled ZPL photons be detected and indistinguishable. We note that the GaP-on-diamond system is compatible with waveguide-coupled superconducting detectors, a technology which has already demonstrated detection efficiencies exceeding 90% for waveguide-coupled photons [24,25].

The demonstrated Purcell factors, as high as 26, exceed what has been achieved in all-diamond waveguide-integrated platforms [20,40]. This suggests that the primary disadvantage of the hybrid-material system for MBQIP, namely that the emitter cannot be placed at the guided-mode maximum, can be largely overcome with continued improvements in resonator quality factor. A greater challenge for all integrated platforms is the production of indistinguishable photons. Specifically, it will be necessary to improve the spectral stability of near-surface NV centers, which currently exhibit spectral diffusion up to 10 GHz [29]. We are encouraged by recent work in improving NV spectral stability via high-temperature annealing [41] and longer-wavelength excitation [10]. Moreover, even if device-integrated NV centers do not exhibit the spectral stability observed for bulk NV centers incorporated during diamond growth, the platform is compatible with Stark tuning for both active ZPL frequency stabilization [42] and tuning to a single platform resonance [9,43].

TABLE I. Summary of key values for four selected devices.

Device	$\gamma_{\text{tot}}(s^{-1})$	$\gamma_{wg}(s^{-1})$	η_1	F_P	η_{out}	η_2	$g^{(2)}(0)$
Disk 1	2.85×10^7	2.48×10^6	9%	26	20%	9%	0.30
Disk 2	2.15×10^7	2.17×10^6	10%	16	23%	8%	0.36
Disk 3	1.85×10^7	1.48×10^6	8%	12	12%	3%	0.19
Disk 4	2.49×10^7	9.72×10^5	4%	16	12%	4%	0.31

We conclude with an outlook for scalability. Our yield for simple photonic circuits which couple the ZPL emission from a single NV center to a single-mode waveguide, and which outperform the theoretical limit for free-space collection, exceeds 10%. This yield is predominantly limited by the yield in NV-resonator coupling, which in the short term can be improved by increasing the density of near-surface NV centers. Longer-term, aligned implantation [44], combined with on-chip switching for device postselection, should enable deterministic coupling of high-performing devices. For the latter approach, the second-order optical nonlinearity associated with GaP can be leveraged to implement integrated electro-optic switching. Thus, we believe the high total quantum efficiency η, combined with large-scale integration demonstrated in this work, is a promising step toward quantum photonic networks in the hybrid GaP-on-diamond platform.

This material is based upon work supported by the National Science Foundation under Grant No. 1506473. We would like to acknowledge I. R. Christen for assistance with graphics, I. R. Christen, S. Chakravarthi for passive device testing, Y. Zhou for FDTD simulations of fabricated devices, and R. Bojko for *e*-beam lithography support. Devices were fabricated at the Washington Nanofabrication Facility, a part of the National Nanotechnology Coordinated Infrastructure network.

[1] M. V. Gurudev Dutt, L. Childress, L. Jiang, E. Togan, J. Maze, F. Jelezko, A. S. Zibrov, P. R. Hemmer, and M. D. Lukin, Quantum register based on individual electronic and nuclear spin qubits in diamond, Science **316**, 1312 (2007).

[2] G. Waldherr, Y. Wang, S. Zaiser, M. Jamali, T. Schulte-Herbuggen, H. Abe, T. Ohshima, J. Isoya, J. F. Du, P. Neumann, and J. Wrachtrup, Quantum error correction in a solid-state hybrid spin register, Nature (London) **506**, 204 (2014).

[3] M. S. Blok, N. Kalb, A. Reiserer, T. H. Taminiau, and R. Hanson, Towards quantum networks of single spins: Analysis of a quantum memory with an optical interface in diamond, Faraday Discuss. **184**, 173 (2015).

[4] R. Raussendorf and H. J. Briegel, A One-Way Quantum Computer, Phys. Rev. Lett. **86**, 5188 (2001).

[5] S. C. Benjamin, D. E. Browne, J. Fitzsimons, and J. J. L. Morton, Brokered graph-state quantum computation, New J. Phys. **8**, 141 (2006).

[6] Ying Li and Simon C. Benjamin, High threshold distributed quantum computing with three-qubit nodes, New J. Phys. **14**, 093008 (2012).

[7] C. Cabrillo, J. I. Cirac, P. García-Fernández, and P. Zoller, Creation of entangled states of distant atoms by interference, Phys. Rev. A **59**, 1025 (1999).

[8] S. D. Barrett and P. Kok, Efficient high-fidelity quantum computation using matter qubits and linear optics, Phys. Rev. A **71**, 060310(R) (2005).

[9] H. Bernien, B. Hensen, W. Pfaff, G. Koolstra, M. S. Blok, L. Robledo, T. H. Taminiau, M. Marhkham, D. J. Twitchen, L. Childress, and R. Hanson, Heralded entanglement between solid-state qubits separated by three metres, Nature (London) **497**, 86 (2013).

[10] W. Pfaff, B. Hensen, H. Bernien, S. B. van Dam, M. S. Blok, T. H. Taminiau, M. J. Tiggelman, R. N. Schouten, M. Markham, D. J. Twitchen, and R. Hanson, Unconditional quantum teleportation between distant solid-state qubits, Science **345**, 532 (2014).

[11] S. D. Barrett, P. Kok, K. Nemoto, R. G. Beausoleil, W. J. Munro, and T. P. Spiller, A symmetry analyser for non-destructive Bell state detection using weak nonlinearities, Phys. Rev. A **71**, 060302 (2005).

[12] Paul E. Barclay, Kai-Mei C. Fu, Charles Santori, Andrei Faraon, and Raymond G. Beausoleil, Hybrid Nanocavity Resonant Enhancement of Color Center Emission in Diamond, Phys. Rev. X **1**, 011007 (2011).

[13] G. Davies, Vibronic spectra in diamond, J. Phys. C **7**, 3797 (1974).

[14] P. Siyushev, V. Jacques, I. Aharonovich, F. Kaiser, T. Müller, L. Lombez, M. Atatüre, S. Castelletto, S. Prawer, F. Jelezko, and J. Wrachtrup, Low-temperature optical characterization of a near-infrared single-photon emitter in nanodiamonds, New J. Phys. **11**, 113029 (2009).

[15] E. M. Purcell, Spontaneous emission probabilities at radio frequencies, Phys. Rev. **69**, 681 (1946).

[16] Michael Gould, Srivatsa Chakravarthi, Ian R. Christen, Nicole Thomas, Shabnam Dadgostar, Yuncheng Song, Minjoo Larry Lee, Fariba Hatami, and Kai-Mei C. Fu, Large-scale gap-on-diamond integrated photonics platform for NV center-based quantum information, J. Opt. Soc. Am. B **33**, B35 (2016).

[17] Marko Loncar and Andrei Faraon, Quantum photonic networks in diamond, MRS Bull. **38**, 144 (2013).

[18] M. J. Burek, Y. W. Chu, M. S. Z. Liddy, P. Patel, J. Rochman, S. Meesala, W. Hong, W. M. Quan, M. D. Lukin, and M. Locar, High quality-factor optical nanocavities in bulk single-crystal diamond, Nat. Commun. **5**, 5718 (2014).

[19] Behzad Khanaliloo, Matthew Mitchell, Aaron C. Hryciw, and Paul E. Barclay, High-q/v monolithic diamond microdisks fabricated with quasi-isotropic etching, Nano Lett. **15**, 5131 (2015).

[20] A. Faraon, C. Santori an Z. Huang, K.-M. C. Fu, V. M. Acosta, D. Fattal, and R. G. Beausoleil, Quantum photonic devices in single-crystal diamond, New J. Phys. **15**, 025010 (2013).

[21] Birgit J. M. Hausmann, Brendan Shields, Qimin Quan, Patrick Maletinsky, Murray McCutcheon, Jennifer T. Choy, Tom M. Babinec, Alexander Kubanek, Amir Yacoby, Mikhail D. Lukin, and Marko Loncar, Integrated diamond networks for quantum nanophotonics, Nano Lett. **12**, 1578 (2012).

[22] D. F. Nelson and E. H. Turner, Electro-optic and piezoelectric coefficients and refractive index of gallium phosphide, J. Appl. Phys. **39**, 3337 (1968).

[23] J. P. Sprengers, A. Gaggero, D. Sahin, S. Jahanmirinejad, G. Frucci, F. Mattioli, R. Leoni, J. Beetz, M. Lermer, M. Kamp, S. Hofling, R. Sanjines, and A. Fiore, Waveguide superconducting single-photon detectors for integrated quantum photonic circuits, Appl. Phys. Lett. **99**, 181110 (2011).

[24] Mohsen K Akhlaghi, Ellen Schelew, and Jeff F Young, Waveguide integrated superconducting single-photon detectors implemented as near-perfect absorbers of coherent radiation, Nat. Commun. **6**, 8233 (2015).

[25] W. H. P. Pernice, C. Schuck, O. Minaeva, M. Li, G. N. Goltsman, A. V. Sergienko, and H. X. Tang, High-speed and high-efficiency travelling wave single-photon detectors embedded in nanophotonic circuits, Nat. Commun. **3**, 1325 (2012).

[26] E. Yablonovitch, D. M. Hwang, T. J. Gmitter, L. T. Florez, and J. P. Harbison, Van der Waals bonding of GaAs epitaxial liftoff films onto arbitrary substrates, Appl. Phys. Lett. **56**, 2419 (1990).

[27] Nicole Thomas, Russell J. Barbour, Yuncheng Song, Minjoo Larry Lee, and Kai-Mei C. Fu, Waveguide-integrated single-crystalline gap resonantors on diamond, Opt. Express **22**, 13555 (2014).

[28] See Supplemental Material at http://link.aps.org/supplemental/10.1103/PhysRevApplied.6.011001 for additional information on the sample fabrication and data analysis procedures.

[29] K.-M. C. Fu, C. Santori, P. E. Barclay, and R. G. Beausoleil, Conversion of neutral nitrogen-vacancy centers to negatively charged nitrogen-vacancy centers through selective oxidation, Appl. Phys. Lett. **96**, 121907 (2010).

[30] F. Jelezko and J. Wrachtrup, Single defect centres in diamond: A review, Phys. Status Solidi (a) **203**, 3207 (2006).

[31] Thomas Oeckinghaus, Rainer Stöhr, Roman Kolesov, Julia Tisler, Friedemann Reinhard, and Jörg Wrachtrup, A compact, diode laser based excitation system for microscopy of NV centers, Rev. Sci. Instrum. **85**, 073101 (2014).

[32] David A. Turton, Gavin D. Reid, and Godfrey S. Beddard, Accurate Analysis of Fluorescence Decays from Single Molecules in Photon Counting Experiments, Anal. Chem. **75**, 4182 (2003).

[33] G. Liaugaudas, G. Davies, K. Suhling, R. U. A. Khan, and D. J. F. Evans, Luminescence lifetimes of neutral nitrogen-vacancy centres in synthetic diamond containing nitrogen, J. Phys. Condens. Matter **24**, 435503 (2012).

[34] A Batalov, C Zierl, T Gaebel, P Neumann, I-Y Chan, G Balasubramanian, P R Hemmer, F Jelezko, and J Wrachtrup, Temporal Coherence of Photons Emitted by Single Nitrogen-Vacancy Defect Centers in Diamond Using Optical Rabi-Oscillations, Phys. Rev. Lett. **100**, 077401 (2008).

[35] A. T. Collins, M. F. Thomaz, and M. I. B. Jorge, Luminescence decay time of the 1.945 eV centre in type Ib diamond, J. Phys. C **16**, 2177 (1983).

[36] W. Lukosz and R. E. Kunz, Light emission by magnetic and electric dipoles close to a plane interface. I. Total radiated power, J. Opt. Soc. Am. **67**, 1607 (1977).

[37] Lucio Robledo, Hannes Bernien, Toeno van der Sar, and Ronald Hanson, Spin dynamics in the optical cycle of single nitrogen-vacancy centres in diamond, New J. Phys. **13**, 025013 (2011).

[38] N. Aslam, G. Waldherr, P. Neumann, F. Jelezko, and J. Wrachtrup, Photo-induced ionization dynamics of the nitrogen vacancy defect in diamond investigated by single-shot charge state detection, New J. Phys. **15**, 013064 (2013).

[39] N. Bar-Gill, L. M. Pham, A. Jarmola, D. Budker, and R. L. Walsworth, Solid-state electronic spin coherence time approaching one second, Nat. Commun. **4**, 1743 (2013).

[40] Andrei Faraon, Paul E. Barclay, Charles Santori, Kai-Mei C. Fu, and Raymond G. Beausoleil, Resonant enhancement of the zero-phonon emission from a colour centre in a diamond cavity, Nat. Photonics **5**, 301 (2011).

[41] Y. Chu, N. P. de Leon, B. J. Shields, B. Hausmann, R. Evans, E. Togan, M. J. Burek, M. Markham, A. Stacey, A. S. Zibrov, A. Yacoby, D. J. Twitchen, M. Loncar, H. Park, P. Maletinsky, and M. D. Lukin, Coherent optical transitions in implanted nitrogen-vacancy centers, Nano Lett. **14**, 1982 (2014).

[42] V. M. Acosta, C. Santori, A. Faraon, Z. Huang, K.-M. C. Fu, A. Stacey, D. A. Simpson, K. Ganesan, S. Tomljenovic-Hanic, A. D. Greentree, S. Prawer, and R. G. Beausoleil, Dynamic Stabilization of the Optical Resonances of Single Nitrogen-Vacancy Centers in Diamond, Phys. Rev. Lett. **108**, 206401 (2012).

[43] L. C. Bassett, F. J. Heremans, C. G. Yale, B. B. Buckley, and D. D. Awschalom, Electrical tuning of single nitrogen-vacancy center optical transitions enhanced by photoinduced fields, Phys. Rev. Lett. **107**, 266403 (2011).

[44] D. M. Toyli, C. D. Weis, G. D. Fuchs, T. Schenkel, and D. D. Awschalom, Chip-scale nanofabrication of single spins and spin arrays in diamond, Nano Lett. **10**, 3168 (2010).